Inorg. Chem. **2004**, *43*, 8010–8017

Anion Ordering and Defect Structure in Ruddlesden–Popper Strontium Niobium Oxynitrides

Gerard Tobías,[†] Daniel Beltrán-Porter,[‡] Oleg I. Lebedev,[§] Gustaaf Van Tendeloo,[§] Juan Rodríguez-Carvajal,[||] and Amparo Fuertes*,[†]

Institut de Ciència de Materials de Barcelona (CSIC), Campus UAB, 08193 Bellaterra, Spain, Institut de Ciència de Materials de la Universitat de València, P.O. Box 2085, Polígono "La Coma" s/n, 46980 Paterna, Spain, EMAT, University of Antwerp (RUCA), Antwerp, Belgium, and Laboratoire Leon Brillouin (CEA-CNRS), CEA/Saclay, 91191 Gif sur Yvette Cedex, France

Received June 11, 2004

The crystal structure of the $n = 1$ member of the Ruddlesden–Popper family $(SrO)(SrNbO_2N)_n$ was refined by the Rietveld method using neutron powder diffraction data. This complex crystallizes in the *I*4/*mmm* space group with cell parameters $a = 4.0506(2)$ and $c = 12.5936(9)$ Å. The refined composition was $Sr_2NbO_{3.28}N_{0.72}$, which corresponds to a formal oxidation state for Nb of +4.72, meaning 72% Nb(V) and 28% Nb(IV). The nitrogen atoms order in the equatorial sites of the niobium octahedra according to Pauling's second crystal rule as the more charged anion occupies the site showing the larger bond strength sums. Pauling's second crystal rule is shown to be able to predict the distribution of anions in the available crystallographic sites in other mixed anion systems such as oxyhalides with K_2NiF_4 structures and other oxynitrides. The defect structure of the $n = 1$ and $n = 2$ members of the same family was investigated by high-resolution electron microscopy. Recurrent intergrowth along the *c* axis with other Ruddlesden–Popper members ($n = 3$, 4, and perovskite) is observed, resulting in streaking along this direction in the corresponding electron diffraction patterns.

Introduction

The lower thermodynamic stability of metal nitrides relative to oxides frequently results in the use of more complicated preparative methods and the production of air-sensitive samples. Nitrides and oxynitrides are thermodynamically less stable because of the unfavorable electronic affinity of nitrogen (1736 kJ/mol for $N \rightarrow N^{3-}$ vs 601 kJ/mol for $O \rightarrow O^{2-}$)[1] and the high-energy bond of the diatomic molecule (945 kJ/mol for N_2 vs 493 kJ/mol for O_2).[2] As a consequence, the investigation of these compounds is relatively less explored with respect to technological applications of known compounds as well as searches for new phases. However, the similarities in electronegativity, polarizability, ionic radius, and coordination number between oxygen and nitrogen allow for the formation of the same structural types when combined with cations, as well as the mutual substitution of both anions on the same crystallographic sites. This can result in the formation of solid solutions in which the formal valence of one or more cations changes according to the O/N ratio. The design of new nitrides or oxynitrides based on phases and crystal structures already known for oxides is consequently a useful tool for exploring and/or modifying a large variety of physical properties, through the formation of either completely new compounds or solid solutions.

The search for new superconducting compounds containing transition metals other than copper has been an important goal since the discovery of superconductivity in cuprates.[3] One of the most explored classes of compounds are the early transition metal layered oxides with special emphasis on those showing electron configurations complementary to Cu(II)/Cu(III) or Cu(II)/Cu(I), i.e., d^1/d^2 or d^1/d^0 systems, such as Li_xNbO_2[4] and $KCa_2Nb_3O_{10}$.[5] Among nitrides, superconductivity below 25 K has been reported for intercalated

* To whom correspondence should be addressed. E-mail: amparo.fuertes@icmab.es.
[†] Institut de Ciència de Materials de Barcelona (CSIC).
[‡] Universitat de València.
[§] University of Antwerp (RUCA).
[||] Laboratoire Leon Brillouin (CEA-CNRS).

(1) Pearson, G. P. *Inorg. Chem.* **1991**, *30*, 2856.
(2) *Encyclopedia of Materials*; Elsevier: Amsterdam, 2001; Vol. 7, p 6161.
(3) Bednorz, J. G.; Müller, K. A. *Z. Phys. B* **1986**, *64*, 189.

10.1021/ic049236k CCC: $27.50
Published on Web 11/06/2004

zirconium and hafnium nitride halides where the transition metal also shows the electronic configuration d^1/d^0.[6,7] Following these approaches, we have investigated Ruddlesden−Popper strontium niobium oxynitrides containing niobium in the 4+/5+ mixed-valence state (i.e., a d^1/d^0 system). Strontium niobium oxides with a perovskite or a Ruddlesden−Popper structure are known only for $Sr_{1-x}NbO_3$.[8] Ruddlesden−Popper members $(AO)(ABO_3)_n$ with $n = 1$ and 2 in the Sr−Nb−O system have not been reported until now. In such compounds, Nb would show an oxidation state of 4+ that is not stable in air at high temperature, and only the perovskite $Sr_{1-x}NbO_3$ has been prepared using reducing conditions.[8−10] One way to allow the formation of Ruddlesden−Popper strontium niobium phases is to substitute one oxygen per nitrogen atom in each perovskite block, because this substitution formally would lead to the oxidation of Nb^{4+} to the more stable Nb^{5+} as occurs in the perovskite $SrNbO_2N$.[11] Recently, we have reported the preparation of the family of oxynitrides with the general formula $(SrO)(SrNbO_2N)_n$, where n perovskite blocks with composition $[SrNbO_2N]$ intergrow with one [SrO] layer of the sodium chloride type.[12] In this family, the average formal oxidation state for niobium could be tuned according to the N/O ratio or/and the presence of anion vacancies, but magnetic susceptibility measurements for samples synthesized under different conditions did not show any superconducting transition down to 4 K.

Oxynitride perovskites have been investigated by several groups. Marchand et al. reported perovskites of early transition metals such as Ti(IV) ($LaTiO_2N$),[13] Nb(V) ($SrNbO_2N$),[11] Ta(V) ($SrTaO_2N$),[11] and W(VI) (Sr,La)-$WO_{2-x}N_{1+x}$),[14] as well as K_2NiF_4-type phases for Nd_2AlO_3N[15] and Sr_2TaO_3N.[16] More recently, Jansen et al. investigated tantalum oxynitride perovskites ($La_{1-x}Ca_xTaO_{2-x}N_{1+x}$) with application as new nontoxic inorganic pigments.[17] One of the topics attracting much attention in these compounds as well as in other oxynitrides is the order/disorder scheme followed by the two anions on the available crystallographic sites, because this can affect properties including anionic conductivity, electrical properties, metallic conductivity, lithium intercalation capacities, etc., and the driving forces determining the anion distribution have not been completely understood.[18−30]

In this paper, we present neutron diffraction results for Sr_2NbO_3N ($n = 1$) that allow for an understanding of the reasons for the order or disorder followed by anions in oxynitrides as well as in other mixed-anion systems with the K_2NiF_4 structure. We show the general trend that the distribution of anions in the available crystallographic sites takes place according to Pauling's second crystal rule, as the more charged anion occupies the site showing the larger bond strength sums. We also discuss a high-resolution electron microscopy study performed on both $n = 1$ and $n = 2$ compounds that constitutes the first report on the microstructure of perovskite-related oxynitrides. In this study, we observe recurrent intergrowths with other Ruddlesden−Popper members with $n > 2$ ($n = 3$, 4) that indicate the existence of these higher-order phases as extended defects.

Experimental Section

Synthesis. Samples with molar ratios Sr/Nb = 2:1 and Sr/Nb = 3:2 as starting compositions for $Sr_2NbO_{3+x}N_{1-x}$ ($n = 1$) and $Sr_3Nb_2O_{5+x}N_{2-x}$ ($n = 2$) were prepared by high-temperature solid-state reaction in flowing NH_3. The chemicals used were commercially available $SrCO_3$ (Baker, 99.9%), Nb_2O_5 (Aldrich, 99.99%), and NH_3 (Carburos Metálicos, 99.9%). The reactants were pressed into a pellet with a 12-mm-diameter die and then treated under flowing NH_3 (180 cm^3/min) at temperatures between 900 and 1050 °C using thermal cycles of 50 h with intermediate regrinding. The products are air sensitive, and their handling between thermal cycles, and for subsequent characterization, was done in an Ar-filled glovebox. Chemical compositions were determined by plasma absorption and XEDS analyses (for cation contents), elemental analysis (for C and N contents), and TGA experiments performed in O_2 and Ar/H_2.

X-ray and Neutron Diffraction. Routine X-ray diffraction patterns were generally recorded in a Rigaku Rotaflex RU-200B rotating-anode diffractometer using Cu K_α radiation, protecting the samples in some cases with a Kapton film. High-resolution X-ray diffraction patterns were obtained on an INEL curved position-sensitive CPS120 powder diffractometer in a horizontal Debye−Scherrer geometry using a rotating capillary of diameter 0.1 mm

(4) Geselbracht, M. J.; Richardson, T. J.; Stacy, A. M. *Nature* **1990**, *345*, 324.
(5) Takano, Y.; Takayanagi, S.; Ogawa, S.; Yamadaya, T.; Môri, N. *Solid State Commun.* **1997**, *103*, 215.
(6) Yamanaka, S.; Hohetama, K.; Kawaji, H. *Nature* **1998**, *392*, 580.
(7) Fuertes, A.; Vlassov, M.; Beltrán-Porter, D.; Alemany, P.; Canadell; Casañ-Pastor, N.; Palacín, M. R. *Chem. Mater.* **1999**, *11*, 203.
(8) Ridgley, D.; Ward, R. J. *J. Am. Chem. Soc.* **1955**, *77*, 6132.
(9) Hannerz, H.; Svennsson, G.; Istomin, S. Ya.; D'yachenko, O. G. *J. Solid State Chem.* **1999**, *147*, 421.
(10) D'yachenko, O. G.; Istomin, S. Ya.; Abakumov, A. M.; Antipov, E. V. *Inorg. Mater.* **2000**, *36*, 315.
(11) Marchand, R.; Pors, F.; Laurent, Y. *Rev. Int. Hautes Temp. Réfract.* **1986**, *23*, 11.
(12) Tobías, G.; Oró-Solé, J.; Beltrán-Porter, D.; Fuertes, A. *Inorg. Chem.* **2001**, *40*, 6867.
(13) Marchand, R.; Pors, F.; Laurent, Y. *Ann. Chim.* **1991**, *16*, 553.
(14) Marchand, R.; Antoine, P.; L'Haridon, P.; Laurent, Y. European Patent Application EP286503, 1988.
(15) Marchand, R.; Pastuszak, R.; Laurent, Y.; Roult, G. *Rev. Chim. Min.* **1982**, *19*, 684.
(16) Pors, F.; Marchand, R.; Laurent, Y. *Ann. Chim.* **1991**, *16*, 547.
(17) Jansen, M.; Letschert, H. P. *Nature* **2000**, *404*, 980.
(18) Wang, P.; Werner, P.; Gao, L.; Harris, R. K.; Thompson, D. P. *J. Mater. Chem.* **1997**, *7*, 2127.
(19) Lerch, M.; Boysen, H.; Radaelli, P. G. *J. Phys. Chem. Solids* **1997**, *58*, 1557.
(20) Clarke, S. J.; Michie, C. W.; Rosseinsky, M. J. *Chem. Mater.* **2000**, *12*, 863.
(21) Clarke, S. J.; Michie, C. W.; Rosseinsky, M. J. *J. Solid State Chem.* **1999**, *146*, 399.
(22) Clarke, S. J.; Hardstone, K. A.; Michie, C. W.; Rosseinsky, M. J. *Chem. Mater.* **2002**, *14*, 2664.
(23) Kim, Y.; Woodward, P. M.; Baba-Kishi, K. Z.; Tai, C. W. *Chem. Mater.* **2004**, *16*, 1267.
(24) O'Meara, P.; Barker, M. G.; Blake, A. J.; Cooke, P. A.; Gregory, D. H. *J. Mater. Chem.* **2000**, 633.
(25) Fang, C. M.; Orhan, E.; de Wijs, G. A.; Hintzn, H. T.; Groot, R. A.; Marchand, R.; Saillard, J.-Y.; de With, G. *J. Mater. Chem.* **2001**, 1248.
(26) Fang, C. M.; de Wijs, G. A.; de Groot, R. A.; Metselaar, R.; Hintzen, H. T.; de With, G. *Chem. Mater.* **2000**, *12*, 1071.
(27) Lauterbach, R.; Schnick, W. *Solid State Sci.* **2000**, *2*, 463.
(28) Cabana, J.; Rousse, G.; Fuertes, A.; Palacín, M. R. *J. Mater. Chem.* **2003**, *13*, 2402.
(29) Cabana, J.; Ling, C. D.; Oró-Solé, J.; Gautier, D.; Tobias, G.; Adams, S.; Canadell, E.; Palacín, M. R. *Inorg. Chem.* **2004**, *43*, 7050.
(30) Hintzen, H. T.; Metselaar, R.; de With, G. *Tijdsch. Klei, Glas Keram.* **2001**, *22*, 19.

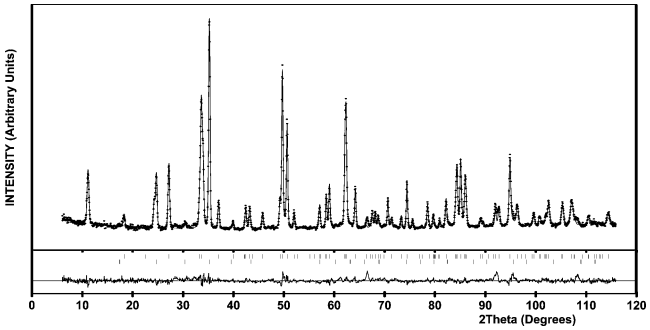

Figure 1. Observed, calculated, and difference neutron diffraction patterns for $Sr_2NbO_{3.28}N_{0.72}$. The impurity phase is the perovskite $SrNbO_2N$.[11]

as the sample holder. The angular range was 120°, and the radiation was Cu Kα_1 (λ = 1.540598 Å), obtained with a Ge(111) monochromator. Samples were sieved to 65 μm and mixed with glass powder before being used to fill the capillary that was sealed under argon.

Neutron powder diffraction data were collected at the high-resolution powder diffractometer 3T2. This diffractometer is installed in the reactor hall of the ORPHEE reactor (Laboratoire Léon Brillouin, Saclay, France). It uses a focusing Ge monochromator providing neutrons of wavelength 1.2253 Å at a takeoff angle $2\theta_M = 91°$. The detector bank has 20 ^{3}He detectors and 20 Soller collimators of 10′ divergence. The resolution function of the diffractometer was calculated using a standard cubic sample free from size and strain broadening. The diffraction data were collected at room temperature using a sealed vanadium can as the sample holder. The treatment of the powder diffraction data was performed using the Rietveld method,[31] as implemented in the program FullProf.[32]

High-Resolution Electron Microscopy. Samples for transmission electron microscopy (TEM) were prepared by crushing the powder in hexane and dispersing the solution on a holey carbon film. Electron diffraction (ED) and high-resolution electron microscopy (HREM) were performed using a JEOL 4000EX microscope operating at 400 kV with a Scherzer resolution limit of 1.7 Å. Computer-simulated images for different defocusing and different thicknesses were obtained using the Crystalkit and MacTempas programs.

Results and Discussion

Neutron Diffraction Refinement of $Sr_2NbO_{3+x}N_{1-x}$. The observed and calculated neutron diffraction patterns for $Sr_2NbO_{3+x}N_{1-x}$ are shown in Figure 1. Table 1 lists the crystallographic and refinement data. As starting coordinates and crystal parameters for this refinement, we used the parameters previously obtained by the Rietveld method from powder X-ray diffraction data.[12] The structure was refined in the space group *I*4/*mmm* that was obtained by electron diffraction from the reconstruction of the reciprocal lattice. Site occupancy factors were fixed to 1 for Nb and refined for the other atoms. Occupancies for Sr and O(2) did not deviate from the initial value after refinement, and consequently, they were fixed to 1 in subsequent cycles. To evaluate the sensitivity of the method for the determination of N positions, we calculated neutron diffraction patterns

Table 1. Crystallographic and Neutron Diffraction Refinement Data for $Sr_2NbO_{3.28}N_{0.72}$

Crystal Data

space group	*I*4/*mmm* (No. 139)	*a* (Å)	4.0506(2)
		c (Å)	12.5936(9)
Z	2		

Atom Coordinates

atom	site	*x*/*a*	*y*/*b*	*z*/*c*	occ
Nb	2a	0	0	0	1
Sr	4e	0	0	0.3532(3)	1
N(1)	4c	0	0.5	0	0.36(3)
O(1)	4c	0	0.5	0	0.64(3)
O(2)	4e	0	0	0.1604(6)	1

Temperature Factors

	$10^3\beta_{11}$	$10^3\beta_{22}$	$10^4\beta_{33}$	B_{eq} (Å^2)
Nb	7(2)	7(2)	6(3)	0.42
Sr	16(2)	16(2)	10(3)	0.87
O,N(1)	7(3)	4(3)	14(3)	0.54
O(2)	26(3)	26(3)	21(9)	1.59

Selected Bond Distances (Å)

d(Nb−N,O(1)) (×4)	2.025	*d*(Sr−O(2)) (×1)	2.428(9)
d(Nb−O(2)) (×2)	2.020(9)	*d*(Sr−O(2)) (×4)	2.8693(6)
d(Sr−O,N(1)) (×4)	2.743(3)		

Refinement Data

λ (Å)	1.2253		
2θ range (deg), step (deg)	$6 \le 2\theta \le 116$, 0.05		
N_p, N_{refln}[a]	2200	133	
P_p, P_i, P_g[b]	11	12	1
R_{Bragg}, R_F, χ^2	3.3	4.9	2.8
R_p, R_{wp}, R_{exp}[c]	14.1	12.5	7.48
f_P[d]	2.9		

[a] N_p and N_{refln} refer to the number of experimental points and the total number of reflections. [b] P_p, P_i, and P_g refer to the number of profile, intensity-dependent, and globally refined parameters, respectively. The profile fitting of the data was performed with a pseudo-Voigt function, including asymmetry and preferred orientation corrections. Preferred orientation and asymmetry were corrected by the March−Dollase and Berar−Bardinozzi expressions, respectively. [c] Conventional Rietveld *R* factors (R_p, R_{wp} R_{exp}) were calculated by using background corrected counts (see ref 32 for definitions). [d] Standard deviations in the table are multiplied by the Pawley parameter f_P (to obtain realistic values) (see ref 32).

(using λ = 1.2253 Å) for two structural models: (I) placing the N atoms in the equatorial site (4c) and (II) placing the N atoms in the axial site (4e) of the niobium octahedron. In these calculations, we used the profile parameters obtained by refinement in the experimental pattern. Results are shown in Figure 2, where the experimental pattern has also been included for comparison. The reflections more affected by the position of N atoms are indicated by arrows. The intensities of reflections 002, 110, 022, 116, 130, and 136 are very sensitive to the position of N atoms because the corresponding crystallographic planes contain either the 4c sites [planes (002) and (022)] or the 4e sites [planes (110), (116), (130), and (136)]. The higher scattering length of N (9.36 fm) relative to O (5.81 fm) leads to an increase of the intensities of reflections 002 and 022 when this atom is placed in the equatorial site and to an increasing of intensities of reflections 110, 116, 130, and 136 when it is placed in the axial sites. The comparison of these patterns with the experimental one—as well as subsequent refinement with both structural models—allows N to be located unambiguously at the equatorial sites (site 1). Occupancies of N and

(31) Rietveld, H. M. *Acta Cryst*. **1967**, *22*, 151.
(32) Fullprof 2000. See http://www-llb.cea.fr/fullweb/powder.htm. Rodríguez-Carvajal, J. *Physica B* **1993**, *192*, 55.

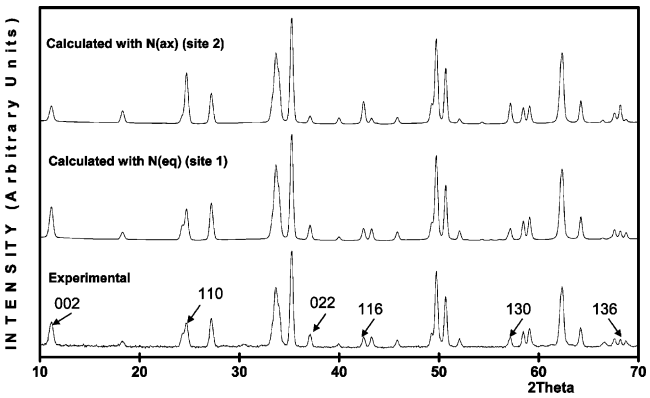

Figure 2. Calculated neutron diffraction patterns for $Sr_2NbO_{3.28}N_{0.72}$ with N atoms placed in the equatorial and axial positions of the niobium octahedron. The experimental pattern is shown at the bottom, with arrows indicating the reflections that are more affected by the position of N atoms.

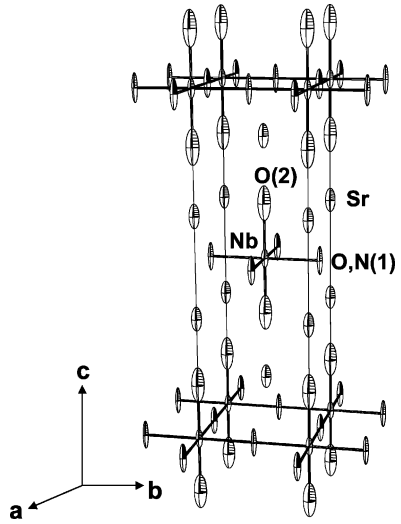

Figure 3. ORTEP diagram of the unit cell for $Sr_2NbO_{3.28}N_{0.72}$ showing 75% ellipsoids.

O atoms were constrained to be complementary in this site and were refined to the values 0.36(3) and 0.64(3), respectively. The perovskite $SrNbO_2N$ was introduced into the refinement as a second phase[11] to account for an impurity peak around $2\theta = 30°$. Other possible second phases—for instance, Ruddlesden−Popper members with $n > 1$ or binary or ternary strontium niobium oxides—were not detected in this sample. A perspective view of the obtained structural model is drawn in Figure 3. The refined composition was $Sr_2NbO_{3.28}N_{0.72}$ and corresponds to a formal oxidation state for Nb of +4.72, meaning 72% Nb(V) and 28% Nb(IV). The presence of Nb(IV) was previously observed by SQUID measurements in a sample synthesized under the same conditions.[12] For this sample, we proposed the stoichiometry $Sr_2NbO_{2.8}N$ obtained by chemical analysis, differing in the O and N contents from the stoichiometry obtained by neutron diffraction in this work but leading to a similar average formal oxidation state for niobium, i.e., +4.6. Discrepancies in the N and O contents between chemical analysis and neutron diffraction are probably caused by the presence of the impurity phase $SrNbO_2N$. The perovskite $SrNbO_2N$ shows a higher N content than the $n = 1$ compound (calculated N compositions $Sr_2NbO_{3.28}N_{0.72}$ 3.05%, $SrNbO_2N$ 6.18%; observed N content from chemical analysis 4.08%). This impurity has been observed in samples of $Sr_2NbO_{3+x}N_{1-x}$ and $Sr_3Nb_2O_{5+x}N_{2-x}$ as intergrowth domains by high-resolution electron microscopy (see below). The partial reduction of Nb(V) to Nb(IV) during the ammonolysis reaction is due to the presence of H_2 as a product of the dissociation of ammonia at temperatures above 500 °C.

The bond distances observed for $Sr_2NbO_{3.28}N_{0.72}$ in the present work are very close to those previously obtained by Rietveld refinement using X-ray powder diffraction data.[12] In the previous study, the N atoms were placed at the equatorial positions by analogy with the results on the isostructural compound Sr_2TaO_3N.[33] The bond distances observed around Nb or Sr are very close to those of Sr_2TaO_3N, in agreement with the similar ionic radii for Nb(V) and Ta(V).[34] Differences larger than 0.5% can be found only in the Sr−O,N bond distances along the *c* axis [Sr_2TaO_3N, d(Sr−O(2)) = 2.728(1) and d(Sr−O,N(1)) = 2.451(1) Å; $Sr_2NbO_{3.28}N_{0.72}$, d(Sr−O(2))= 2.743(1) and d(Sr−O,N(1))= 2.428(3) Å]. These small differences could be a consequence of the higher content of N (with an ionic radius larger than oxygen) in the tantalum compound. The bond distances around the transition metals are the same for both compounds. In this case, the presence in $Sr_2NbO_{3.28}N_{0.72}$ of some Nb(IV), with an ionic radii slightly larger than that of Nb(V) (0.68 vs 0.64 Å), would compensate for the effect caused by the lower N content, resulting nearly identical Nb−O,N and Ta−O,N bond distances. In contrast to $Sr_2NbO_{3.28}N_{0.72}$, the stoichiometry for the tantalum compound was found to be close to the ideal Sr_2TaO_3N by both neutron refinement and TGA methods,[22,33] the lower N/O ratio in the niobium compound originating from the higher reducibility of this metal compared to tantalum under the synthesis conditions.

High-Resolution Electron Microscopy. To understand the microstructure of the Ruddlesden−Popper [SrO]-[$SrNbO_2N$]$_n$ family, several samples of the $n = 1$ and $n = 2$ members were studied by ED and HREM. A high-resolution electron microscopy image along [010] zone axis for the $n = 1$ compound is shown in Figure 4a. The calculated images, using the crystal parameters of Table 1, for different defocus values and thicknesses are in good agreement with the experimental images. One of them, for a defocus of 57 nm and a thickness of 7 nm, is included as an inset. The intense bright dots correspond to the Sr configuration, and the less intense dots are assigned to the Nb atoms. A schematic representation of the $n = 1$ simulated image is shown in Figure 4c. The Sr atoms are represented by black dots, and the Nb atoms are placed in the center of the octahedrons. $n = 1$ samples are mostly free of defects, but some crystals show a variety of defects resulting in streaking along the *c* axis in the electron diffraction pattern (Figure 4b). In most of these cases, we observed by HREM recurrent intergrowth along the *c* axis with other Ruddlesden−Popper members, as shown in Figure 5. These defects

(33) Diot, N.; Marchand, R.; Haines, J.; Léger, J. M.; Macaudière, P.; Hull, S. *J. Solid State Chem.* **1999**, *146*, 390.
(34) Shannon, R. D. *Acta Crystallogr. A* **1976**, *32*, 751.

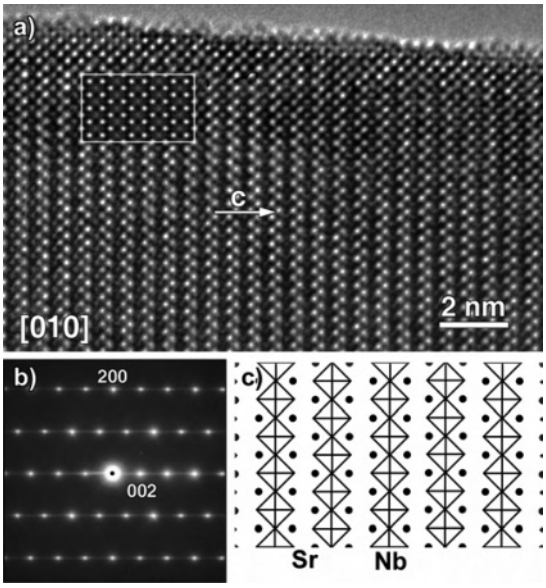

Figure 4. (a) High-resolution electron microscopy image along [010] for the compound Sr_2NbO_3N. The calculated image for a defocus of 570 Å and a thickness of 70 Å model is shown as an inset. (b) ED pattern. (c) Schematic representation of the simulated region.

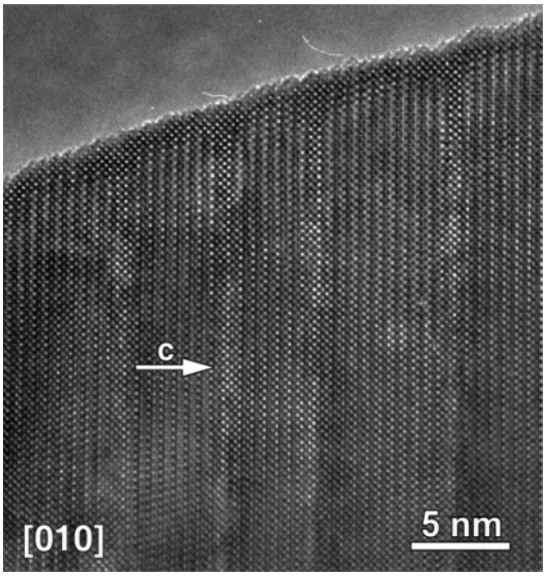

Figure 5. High-resolution electron microscopy image of recurrent intergrowth with other Ruddlesden−Popper members in Sr_2NbO_3N.

allow for the accommodation of local deviations from the nominal stoichiometry and are generally observed in Ruddlesden−Popper oxides.[35] In Figure 6a, we show an example of such intergrowth; step boundaries (indicated by arrowheads) are common features for these structures. One of these step boundaries was analyzed in detail (Figure 6b). The simulated image for a thickness of 8 nm and a defocus of 57 nm is presented in Figure 6c. For these parameters, the intense bright dots correspond to the Sr configuration and the less bright dots to the Nb atoms. In the schematic representation of this image (Figure 6d), we have identified the intergrowth of the $n = 2-4$ members of the family $[SrO]-[SrNbO_2N]_n$. They are labeled as $p = 2$, 3, and 4, respectively, and are local domains that can be thought off as perovskite regions of width p (p refers to perovskite). We did not find large regions with $1 < n \leq 4$ in the Sr_2NbO_3N samples. Because of the absence of crystallographic data for the members $n = 2-4$, we performed image simulation using structural models in analogy with the structure of the $n = 1$ member. A defect that is even more frequent is the intergrowth of cubic perovskite domains as shown in Figure 7. The best correspondence to this experimental image was obtained using a defocus of 57 nm and a thickness of 5 nm. In this case, the bright dots correspond to both Sr and Nb atoms. The schematic structure is presented as an inset. In this scheme, the Sr atoms are represented as black dots, and the Nb atoms are placed in the middle of the octahedron.

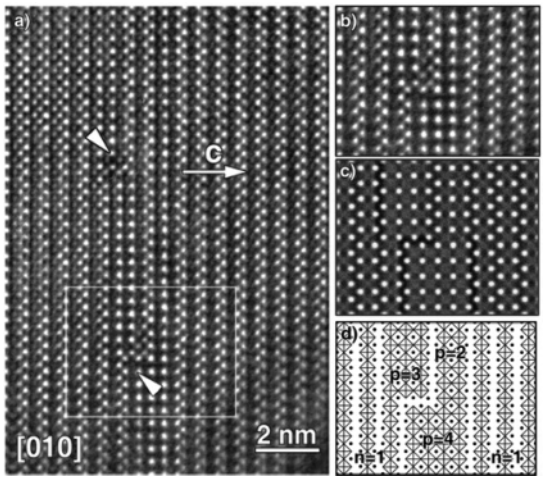

Figure 6. (a) High-resolution electron microscopy image showing step intergrowth boundaries between domains of $n = 2-4$ Ruddlesden−Popper members within a crystal of the $n = 1$ phase. (b) Detail of an step intergrowth boundary. (c) Simulated image for a thickness of 80 Å and a defocus of 570 Å. (d) Schematic representation of the detail region.

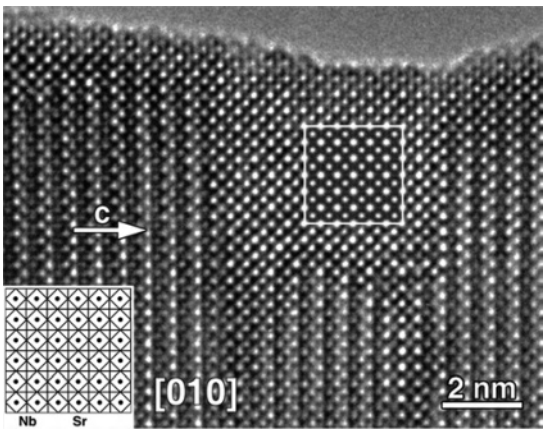

Figure 7. High-resolution electron microscopy image of perovskite ($SrNbO_2N$) domains within a crystal of the $n = 1$ phase. The simulated image (defocus of 570 Å, thickness of 50 Å) and schematic representation are shown as an inset.

Figure 8 shows an HREM image of the $n = 2$ member along the [010] zone axis. On the left side, the characteristic contrast for this phase is observed, whereas on the right side, a domain with the characteristic contrast of the cubic perovskite structure ($n = \infty$) is imaged. The coexistence of the $n = 2$ member and perovskite in the same crystal is also

(35) Sloan, J.; Battle, P. D.; Green, M. A.; Rosseinsky, M. J.; Vente, J. F. *J. Solid State Chem.* **1998**, *138*, 135.

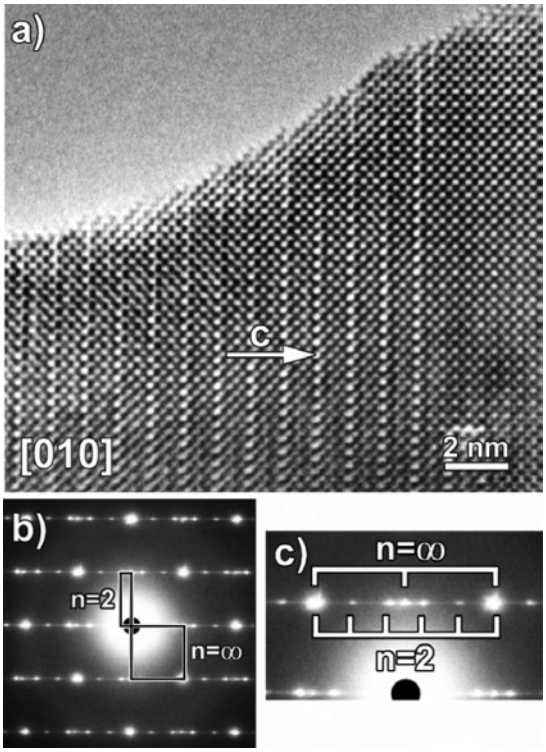

Figure 8. (a) High-resolution electron microscopy image of the $n = 2$ member along the [010] zone axis. (b) ED pattern. (c) Assignment of the reflections corresponding to $n = 2$ and perovskite phases.

observed in the electron diffraction pattern (Figure 8b), where it is possible to assign reflections corresponding to both phases (Figure 8c).

The presence of perovskite domains in both $n = 1$ and $n = 2$ members can be explained by assuming local deviations from the nominal stoichiometry in the samples as well as considering the reaction pathway followed by these phases during their synthesis. We have performed X-ray diffraction and electron diffraction studies on samples obtained at different temperatures and treatment times, and in both $n = 1$ and $n = 2$ compounds, the reaction proceeds with increasing the complexity of the phases, through the formation of $SrNbO_2N$ as a first step at 950 °C. Further heating at 1050 °C leads first to the formation of Sr_2NbO_3N and finally to the $n = 2$ member.[36]

Anion Ordering and the Application of Pauling's Second Crystal Rule. $Sr_2NbO_{3.28}N_{0.72}$ represents a new example of oxynitride showing the partial ordering of nitrogen and oxygen. The distribution of the anions is identical to that of the homologous tantalum compound, Sr_2TaO_3N, with nitrogen occupying the equatorial sites of the perovskite octahedron. The approximate composition and sequence of the layers along the *c* axis for both compounds is then [SrO]−[MNO]−[SrO]−[SrO]−[MNO]− ··· (M = Nb, Ta).

To understand the reasons for the observed anion ordering scheme in these compounds, we calculated the bond strength sums for each anionic position using the equation of Pauling's second crystal rule (PSCR)[37]

$$\sum_i \frac{z_i}{\nu_i} = \sum_i s_i$$

where z_i is the electric charge of each cation bonded to a given anionic position and ν_i is its coordination number. Pauling's second crystal rule states that these sums must be approximately equal to the electric charge, ζ, of the anion occupying the position. We have calculated also these sums for other oxynitrides as well as for representative K_2NiF_4-type compounds containing oxygen and other anions, in particular oxychlorides and oxyfluorides. Table 2 compare the values obtained in the different compounds as well as the Pauling electronegativities (χ)[38] of the elements involved in each case. A trend for the compounds in this table, regardless of the constituent anions, is that, when ordering occurs, the more electronegative anion is preferentially coordinated to the more electropositive metal. This is the case for the tantalum and niobium oxynitrides with the K_2NiF_4 structure, where N occupies the in-plane positions of the octahedra. In these sites, the anion is coordinated to two transition metals and four alkaline-earth cations, whereas in the axial positions, they are coordinated to one transition metal and five alkaline-earth metals. A different ordering occurs in the oxyfluorides showing the same structural type. In $Sr_2CuO_2F_2$, K_2NbO_3F, and Ba_2InO_3F, the fluorine occupies the axial positions, where it is preferentially coordinated to the more electropositive cation. However, there are some examples where the differences in electronegativities do not explain the observed arrangement of cations and anions. For instance, the compounds Sr_2MnO_3Cl, Sr_2CoO_3Cl, and Nd_2AlO_3N show a distorted K_2NiF_4 structure with symmetry *P*4/*nmm*, where the chlorine or nitrogen occupies one of the two axial positions of the octahedra and oxygen atoms lie at the other axial site as well as in the equatorial positions. In Nd_2AlO_3N, the difference between the electronegativities of Nd and Al is small, and this could explain why the observed ordering differed from that expected according to this criterion, but for the two oxychlorides, the transition metals have electronegativities similar to those of tantalum and

(36) Tobías, G. New Layered Oxynitrides of Niobium and Tantalum and Related Systems: Synthesis, Crystal Chemistry and Electronic Structure. Ph.D. Thesis, Autonomous University of Barcelona, Barcelona, Spain, 2004.

(37) Pauling, L. *J. Am. Chem. Soc.* **1929**, *51*, 1010.
(38) Pauling, L. *Uniones Químicas* (*The Nature of the Chemical Bond*), Kapelusz S.A.: Buenos Aires, Argentina, 1965 (in Spanish).
(39) Knee, C. S.; Zhukov, A. A.; Séller, M. T. *Chem. Mater.* **2002**, *14*, 4249.
(40) Loureiro, S. M.; Felser, C.; Huang, Q.; Cava, R. J. *Chem. Mater.* **2000**, *12*, 3181.
(41) Al-Mamouri, M.; Edwards, P. P.; Greaves, C.; Slaski, M. *Nature* **1994**, *369*, 382.
(42) Galasso, F.; Darby, W. *J. Phys. Chem.* **1962**, *66*, 1318.
(43) Needs, R. L.; Weller, M. T.; Scheler, U.; Harris, R. K. *J. Mater. Chem.* **1996**, *6*, 1219.
(44) Gudat, A.; Hagg, S.; Kniep, R.; Rabenau, A. *Z. Naturforsch. B* **1990**, *45*, 111.
(45) Chen, X. Z.; Eick, H. A. *J. Solid State Chem.* **1996**, *127*, 19.
(46) O'Meara, P. M.; Barker, M. G.; Blake, A. J.; Cooke, P. A.; Gregory, D. H. J. *Chem. Soc., Dalton. Trans.* **2000**, 633.
(47) Hochreim, O.; Kniep, R. *Z. Anorg. Allg. Chem.* **2001**, *627*, 301.
(48) Armytage, D.; Fender, B. E. F. *Acta Crystallogr.* **1974**, *B30*, 809.
(49) Weshaupt, M.; Strähle, J. *Z. Anorg. Allg. Chem.* **1977**, *429*, 261.

Table 2. Bond Strength Sums and Electronegativities in Oxynitrides and Oxyhalides

compound	structural type, space group	ordering scheme or coordination preferences	Pauling electronegativities[a]	$\bar{\zeta}$[b]	bond strength sums (PSCR) for anion sites	ref(s)
Sr_2TaO_3N	K_2NiF_4 *I*4/*mmm*	O_{axial}, $[N,O]_{equat}$	Sr 1.0, Ta 1.5	2.25	axial 1.94 equat. 2.55	33, 22
Ba_2TaO_3N	K_2NiF_4 *I*4/*mmm*	O_{axial}, $[N,O]_{equat}$	Ba 0.9, Ta 1.5	2.25	axial 1.94 equat. 2.56	22
$Sr_2NbO_{3.28}N_{0.72}$	K_2NiF_4 *I*4/*mmm*	O_{axial}, $[N,O]_{equat}$	Sr 1.0, Nb 1.6	2.18	axial 1.94 equat 2.56	this work
Nd_2AlO_3N	K_2NiF_4 *P*4/*nmm*	$[N,O]_{axial}$, O_{equat}	Nd 1.2, Al 1.5	2.25	axial 2.17 equat 2.33	15
Sr_2MnO_3Cl	K_2NiF_4 *P*4/*nmm*	$[Cl,O]_{axial}$, O_{equat}	Sr 1.0, Mn 1.5, Cl 3.0	1.75	axial 1.61 equat 1.88	39
Sr_2CoO_3Cl	K_2NiF_4 *P*4/*nmm*	$[Cl,O]_{axial}$, O_{equat}	Sr 1.0, Co 1.8, Cl 3.0	1.75	axial 1.61 equat 1.88	40
$Sr_2CuO_2F_2$	K_2NiF_4 *I*4/*mmm*	F_{axial}, O_{equat}	Sr 1.0, Cu 1.9, F 4.0	1.5	axial 1.44 equat 1.56	41
K_2NbO_3F	K_2NiF_4 *I*4/*mmm*	$[O,F]_{axial}$, O_{equat}	K 0.8, Nb 1.6, F 4.0	1.75	axial 1.38 equat 2.11	42
Ba_2InO_3F	K_2NiF_4 *I*4/*mmm*	$[O,F]_{axial}$, O_{equat}	Ba 0.9, In 1.7, F 4.0	1.75	axial 1.61 equat 1.88	43
$Li_{14}Cr_2N_8O$	antifluorite $P\bar{3}$	Li−O,N; Cr−N	Li 1.0, Cr 1.6	2.89	N1,N2 3; O 2	44
$Li_{16}Nb_2N_8O$	antifluorite $P\bar{3}$	Li−N,O; Nb−N	Li 1.0, Nb 1.6	2.89	N1,N2 3; O 2	45
Sr_4MoN_4O	layered $P2_1/m$	Sr−O, Mo−N	Sr 1.9, Mo 1.8	2.80	N 3.07, 2.83, 3.12, 2.74, 2.45, 2.5 O 1.95, 2.0	46
$Li_6Ca_{12}Re_4N_{16}O_3$	modified Th_3P_4	Li−N,O; Ca−N,O; Re−N	Li 1.0, Ca 1.0, Re 1.9	2.84	N1 3.10 N2 3.03 O 1.73	47
TaON	Baddeleyite $P2_1/c$	Ta−O, Ta−N	Ta 1.5	2.5	O 2.14 N 2.86	48
NbON	Baddeleyite $P2_1/c$	Nb−O Nb−N	Nb 1.6	2.5	O 2.14 N 2.86	49

[a] $\chi(O) = 3.5$, $\chi(N) = 3.0$. [b] Average charge of anions.

niobium and the electronegativity of chlorine is the same as that for nitrogen.

A different explanation of the observed ordering can generally be based on the bond strength sums and the tendency to satisfy Pauling's second crystal rule. Except for Nd_2AlO_3N, in all of the K_2NiF_4-type compounds of Table 2, the more charged anion occupies the site with the larger PSCR bond strength sum. Pauling's second crystal rule is well satisfied in the tantalum and niobium compounds with K_2NiF_4 structures because O occupies the axial site with a PSCR sum of 1.94 whereas the equatorial site with the sum of 2.56 is occupied by N and O. Considering the occupancy factors for O and N, the average ζ for the anion in this site is 2.5 for Sr_2TaO_3N or Ba_2TaO_3N and 2.36 for $Sr_2NbO_{3.28}N_{0.72}$. In the oxychlorides and oxyfluorides, the agreement is not generally as good, but the halide always occupies the axial site that has the smaller bond strength sums. In Nd_2AlO_3N, the differences in bond strength sums between the two sites is small, and this could account for the different behavior. We can conclude that, in the K_2NiF_4 structural type, which is anisotropic and has two crystallographically independent and chemically different sites for the anions, it is possible to predict their occupation according to the PSCR. In oxynitrides showing other structural types, the PSCR is generally satisfied,[18,27,44−50] and in most cases, it would allow for the prediction of the positions of the nitrogens in the anion lattice in the absence of neutron diffraction data. In Table 2, we have included several examples of ordered oxynitrides with different transition metals and electropositive elements. To simplify the table, we have selected a representative list of compounds, but many more examples could be included to show the same conclusion: regardless of the structural type and the transition metal, when ordering takes place, the nitrogen atoms occupy the sites with the larger PSCR sums. Bond valence sums (BVSs)[51] are generally more precise for interpreting anion coordination preferences and would have led to similar conclusions, but such calculations require previous knowledge of the crystal coordinates and hence cannot be used with the simplicity and predictive character of PSCR sums, which require only knowledge of the structural type and the available sites for anions. The usefulness of our approach[52] can be shown through one paradigmatic example in which O/N ordering has been the matter of discussion.[25] TaON is a relevant oxynitride because of its application as a very efficient photocatalyst for the oxidation of water into O_2.[53] It is isostructural with baddeleyite (ZrO_2)[48] and exhibits an ordered distribution of N and O between the two available crystallographic sites for anions, A_1 and A_2.[48,25] The two sites exhibit different coordination numbers to cations (4 for site A_1 and 3 for site A_2) and hence different PSCR sums. In the case of TaON, it is clear that an ordered arrangement of N and O is preferred, as the bond strength sums for the two sites are 2.14 (for A_2, O site) and 2.86 (for A_1, N site), in

(50) Morgan, P. E. D. *J. Mater. Sci.* **1986**, 4305.

(51) Brown, I. D.; Shannon, R. D. *Acta Crystallogr.* **1973**, *A29*, 266.

(52) Fuertes, A. Institut de Ciència de Materials de Barcelona (CSIC), Bellaterra, Spain. Unpublished results.

(53) Hitoki, G.; Takata, T.; Kondo, J. N.; Hara, M.; Kobayashi, H.; Domen, K. *Chem. Commun.* **2002**, 1698.

contrast with the same sums corresponding to ZrO_2 (2.29 for A_1 site and 1.70 for A_2 site), where both positions are occupied by oxygen atoms.

Conclusions

The microstructure of the two members of the family $(SrO)(SrNbO_2N)_n$ with $n = 1$ and $n = 2$ show perovskite domains as well as recurrent intergrowths with other Ruddlesden−Popper members with $n > 2$ ($n = 3$, 4) that indicate the existence of these higher-order phases as extended defects. The refined stoichiometry obtained by neutron diffraction for the $n = 1$ compound is $Sr_2NbO_{3.28}N_{0.72}$, indicating a mixed-valence state for niobium, intermediate between +4 and +5 that results from a nitrogen deficiency with respect to the nominal stoichiometry. The nitrogen atoms order in the equatorial sites of the niobium octahedra according to Pauling's second crystal rule, which is shown to be able to predict in a simple way the distribution of anions in oxynitrides as well as in other mixed systems such as oxyhalides with K_2NiF_4 structures.

Acknowledgment. We are grateful to Judith Oró-Solé for performing electron diffraction and low-resolution electron microscopy studies. This work was supported by the Generalitat de Catalunya (Grant 2001SGR 00361) and the Ministerio de Ciencia y Tecnología (Grant MAT 2002-00439). Part of this work was performed within the framework of IAP V-1. G.T. thanks FPI-MCYT for a fellowship.

Supporting Information Available: Crystallographic data in CIF format. This material is available free of charge via the Internet at http://pubs.acs.org.

IC049236K